Korean J. Chem. Eng., 33(11), 3121-3127 (2016)
DOI: 10.1007/s11814-016-0157-8

pISSN: 0256-1115
eISSN: 1975-7220

Effect of gas diffusion layer compression on the polarization curves of a polymer electrolyte membrane fuel cell: Analysis using a polarization curve-fitting model

In-Su Han*, Sang-Kyun Park, and Chang-Bock Chung***,†**

*R&D Center, GS Caltex Corp., 359 Expo-ro, Yusung-gu, Daejeon 34122, Korea
**Division of Marine Information Technology, Korea Maritime and Ocean University, Busan 49112, Korea
***School of Chemical Engineering, Chonnam National University, Gwangju 61186, Korea
(*Received 20 February 2016 • accepted 8 June 2016*)

Abstract−The effect of gas diffusion layer (GDL) compression on the polarization curves of a polymer electrolyte membrane fuel cell was analyzed using a polarization curve-fitting model. The polarization curves measured at four different GDL compression ratios were fitted with the model and were decomposed into an open circuit voltage and three over-voltages resulting from activation, ohmic, and mass-transport losses, respectively. The model fitting was excellent enough to use the model in the subsequent analysis of the GDL compression effect. The relationship between the over-voltages and the compression ratio was investigated by analyzing the estimated model parameters, and an optimal compression ratio was determined for the fuel cell. The proposed analysis method based on the polarization curve-fitting model can be applied to identifying quantitative differences of polarization curves under various operating conditions and designs for fuel cells.

Keywords: Polymer Electrolyte Membrane Fuel Cell, Gas Diffusion Layer, Compression, Polarization Curve, Modeling

INTRODUCTION

A polymer electrolyte membrane (PEM) fuel cell is an electric power generation device that uses proton conductive polymer membranes as the electrolyte and consumes hydrogen and oxygen for electro-chemical reactions [1,2]. Over the last two decades, the design, modeling, and manufacturing technologies of PEM fuel cells have been extensively developed for stationary and mobile applications such as residential power generators, backup power generators, and power generation systems for the propulsion of cars, buses, forklifts, watercraft, and aircraft [3-8]. To facilitate the wide use of the PEM fuel cells for those applications, we should further improve the performance and durability and minimize the manufacturing costs.

Typically, a PEM fuel cell consists of the following major components: membrane-electrode-assemblies (MEAs), gas diffusion layers (GDLs), bipolar-plates, gaskets, and compression plates. A single fuel cell is assembled using these components once or twice, whereas a fuel cell stack is fabricated using them repeatedly. All the components of a fuel cell should be properly combined and tightened using compression plates and bolts both to prevent gas leakage and to lower internal resistance. The compression force on the fuel cell is an important factor for its performance and durability. Weak compression may lead to poor performance owing to high contact resistance, whereas over-compression may result in lower durability owing to the damages to MEAs or GDLs. Therefore, an optimal degree of compression should be determined to achieve the best possible performance and durability of a fuel cell.

The GDLs perform multiple functions in a fuel cell: they diffuse reactant gases to the catalyst layers, remove liquid water, and conduct electrons. Typically, sheets of carbon paper are used as GDLs on both sides of an MEA, and their characteristics vary depending on the degree of compression. In general, as the compression force increases, the contact resistances between the cell components (GDLs-MEAs and GDLs-bipolar plates) decrease, thus lowering ohmic resistance in the fuel cell. In contrast, the pore volume of the GDLs is reduced, thus increasing mass-transport resistance. The degree of GDL compression also affects the open circuit voltage (OCV) and electrochemical reactions in the fuel cell.

Several research groups have addressed the effects of GDL compression on the performance (or polarization curves) of PEM fuel cells. Lee et al. [9] obtained the polarization curves of a PEM fuel cell for three different types of GDLs at two different operating temperatures. The optimal compression torque of the fuel cell was determined from the measured polarization curves. Ge et al. [10] used two different types of GDLs and measured the polarization curves of a single PEM fuel cell using a specifically designed cell fixture for adjusting the compression ratio during experiments. Lin et al. [11] found the optimal compression ratios of a PEM fuel cell by measuring polarization curves for two different types of carbon cloth GDLs. Zhou et al. [12] investigated the effects of compression force on two different GDLs using a computational fluid dynamics (CFD) model. They found that thinner GDLs produced less sensitive performance variations to the compression force than thicker ones. The contact resistances between cell components were experimentally evaluated by several researchers [13-15], and the effects of GDL compression on gas/water transports in PEM fuel cells were investigated by Bazylak et al. [16] and Yee et al. [17]. However, most

†To whom correspondence should be addressed.
E-mail: chungcb@jnu.ac.kr

of the previous studies focused on investigating the overall performance of PEM fuel cells under different GDL compressions rather than on analyzing the respective causes, such as fuel crossover, activation, ohmic, and mass-transport (or concentration) losses, of the performance variations.

In this work, we analyzed the effects of GDL compression on the polarization curves of a PEM fuel cell using a polarization curve-fitting model. Polarization curves were obtained from the experiments of the fuel cell with four different compression ratios and then were fitted using the model. The estimated parameters of the model were used in the subsequent analysis of the effects of GDL compression on the OCV and the activation, ohmic, and mass-transport losses in the fuel cell. In addition, an optimal compression ratio was determined for the PEM fuel cell.

EXPERIMENTAL

A single PEM fuel cell with an active area of 50 cm^2 was fabricated using the following cell components: an MEA (Gore™ 5721), GDLs (SGL™ 10BC), bipolar-plates (the flow-fields of which were machined on graphite-polymer composite plates), and gaskets (made of Teflon sheets). The gaskets were prepared in four different thicknesses of 280, 243, 205, and 167 μm to adjust the compression ratios of the GDLs at 15%, 26%, 36%, and 46%, respectively. The fuel cell was assembled as illustrated in Fig. 1 by clamping all the cell components between two compression plates. Because the gaskets were made of incompressible Teflon sheets, the compression ratio (CR) of the GDLs was determined by the thicknesses of the gaskets according to the following formula:

$$CR = \frac{(t_{GDL} - t_{gasket} - t_{subgasket})}{t_{GDL}} \times 100\% \quad (1)$$

where t_{GDL} is the average thickness of the GDLs before compression, t_{gasket} is the thickness of the gasket, and $t_{subgasket}$ is the thickness of the sub-gasket which protects the edge of the MEA. At first, the fuel cell with the thickest gaskets was assembled and tested for its performance. After the testing, the cell was disassembled to replace the gaskets by the second thickest ones, and then reassembled with all the other components retained. This procedure was repeated four times to cover the four compression ratios mentioned above.

In each performance testing of the fuel cell, the polarization curves, ohmic resistances, alternating current (AC) impedance, and hydrogen crossover currents were measured as follows. First, the fuel cell was activated under the following operating conditions: the hydrogen and air stoichiometries were set at 2.0 and 3.0, respectively, the cell temperature was regulated at 70 °C, the hydrogen and air were fully humidified using a bubbler-type humidifier, and the outlet pressures of both the anode and cathode were kept at atmospheric pressure. The activation was continued until the fuel cell reached the maximum current density at a low cell voltage of 0.5 V. After the activation was complete, the polarization curves and ohmic resistances were measured several times to ensure that the performance of the fuel cell was reproducible under the same operating conditions. The polarization curves were measured with only the hydrogen and air stoichiometries changed to 1.2 and 2.0, respectively, and all the other operating variables fixed. A programmable electrical load (Model 890CL, Scribner Associates) was used to measure the polarization curves by decreasing the cell voltage from the OCV to 0.55 V in 0.025 V step. At every decrement step, the current density was measured for 1 min and averaged over time. The ohmic resistance of the fuel cell was evaluated at the measured points of the current density using a current interrupt testing module equipped in the electrical load. The module computes the ohmic resistance from the voltage gains obtained by interrupting the current for a short period [1,2]. Electrochemical impedance spectroscopy (EIS) [18] was used to measure AC impedance using a frequency response analyzer (Model 880, Scribner Associates) integrated with the electrical load. Impedance spectra were recorded

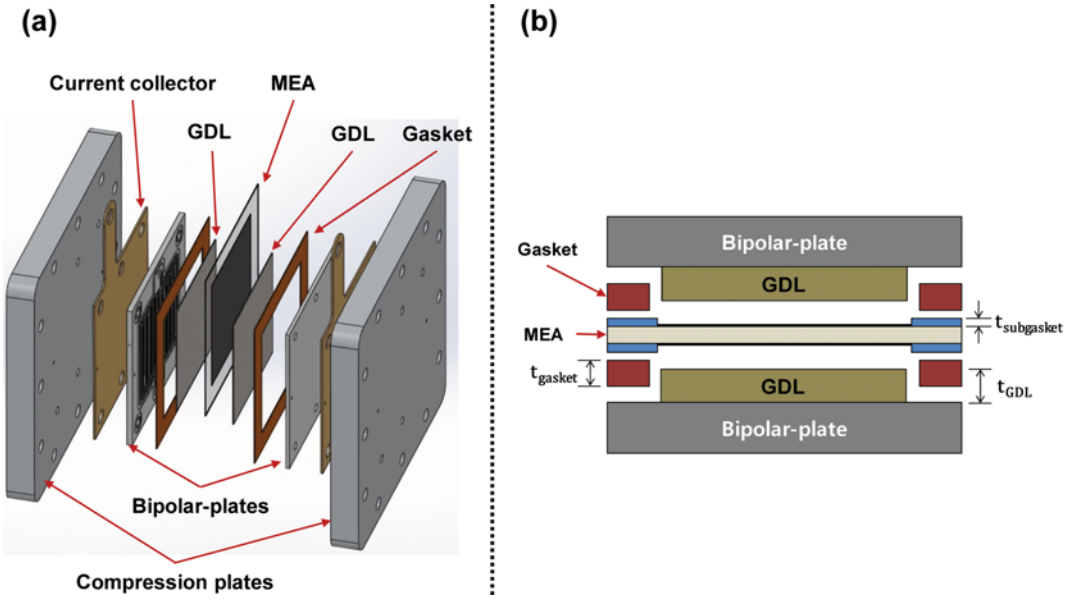

Fig. 1. Structure of the PEM fuel cell: (a) Assembly drawing and (b) cross-sectional view.

as the frequency was scanned from 10 kHz to 0.1 Hz under the same operating conditions used for measuring the polarization curves. Finally, the hydrogen crossover current was measured with a potentiostat (Solartron Model SI 1253, AMETEK) on the basis of linear sweep voltammetry (LSV). LSV has been widely used as a convenient technique to measure the hydrogen crossover rate through the membrane of an MEA in a PEM fuel cell, which is proportional to the crossover current [2]. During the measurement, hydrogen and nitrogen were supplied at 0.57 and 0.63 SLPM (standard liter per minute) to the anode and cathode sides of the fuel cell, respectively. The crossover current was measured while increasing the cell voltage across the two electrodes from 0 to 0.6 V at a constant rate of 1.0 mV s^{-1}.

MODELING AND ANALYSIS METHOD

The polarization curve expresses the relationship between the cell voltage and the current density at a given operating condition and is known as the most representative performance indicator for fuel cells. Because the performance of a PEM fuel cell is affected by various structural and operational parameters, such as the cell design, the cell components, the clamping pressure, the operating temperature and pressure, and the stoichiometries and relative humidities of reactant gases, the polarization curve varies depending on these parameters. The polarization curves at a given operating condition can be fitted using various types of mathematical models, including empirical and semi-empirical equations [19-23].

In this study, the polarization curves measured for the fuel cell with different compression ratios were modeled and analyzed by using the following semi-empirical model, which was originally proposed by Kim et al. [21] and has been found to give excellent fits to the polarization curves of PEM fuel cells [21-23]:

$$V_{cell}=E_0-b\ln(i)-R\,i-p\exp(q\,i) \quad (2)$$

where V_{cell} [V] is the cell voltage, i [mA cm^{-2}] the current density, E_0 [V] the OCV, b [V] the Tafel parameter for oxygen reduction, R [kΩ cm^2] the ohmic resistance, and p [V] and q [cm^2 mA^{-1}] are the diffusion parameters. The first term on the right-hand side of Eq. (2) stands for the OCV, and the other terms represent the over-voltages (or voltage losses). The OCV decreases from its theoretical voltage mainly due to hydrogen crossover and/or internal current, which are caused by the migration of unreacted hydrogen and electrons through the membrane [1]. The second term represents the activation over-voltage that is caused by the slowness of the electro-chemical reactions in the catalyst layers of the MEA. The third term represents the ohmic over-voltage due to the resistance to the electron flow in the electrodes and other electrically conductive components as well as the resistance to the ionic transport through the membrane. Finally, the last term accounts for the mass-transport over-voltage, which is caused by the concentration drop of reactant gases in the catalyst layers. Although the polarization curve-fitting model does not explain microscopic phenomena occurring in the fuel cell, the performance variations due to the changes in the GDL compression can be explicitly analyzed using it. The model has only one independent variable (current density) and five parameters (E_0, b, R, p, and q) to be determined. These parameters were estimated using a nonlinear least-squares fitting algorithm, which was implemented in the MATLAB function (*lsqnonlin*) [24], to best fit the measured polarization curves as follows:

$$\min J(E_0, b, R, p, q)=\Sigma_{k=1}^{n}(V_{cell,k}-V_{cell,k}^{m})^2 \quad (3)$$

where n is the number of measurement points for a polarization curve, and $V_{cell,k}$ and $V_{cell,k}^{m}$ are the calculated and measured cell voltages, respectively, at the measurement point k. The estimated parameters were used to decompose the cell voltage into the OCV and the three over-voltages and thus to analyze the effects of GDL compression.

RESULTS AND DISCUSSION

1. Effects of GDL Compression on the Polarization Curves

Fig. 2 shows the polarization curves along with the ohmic resistances measured at the following four different compression ratios: 15%, 26%, 36%, and 46%. Overall, the changes in the GDL compression ratio had significant effects on the performance of the fuel cell. The OCV was lowered as the compression ratio increased: 1.019, 0.986, 0.953, and 0.929 V for the compression ratios of 15%, 26%, 36%, and 46%, respectively. It indicates that the hydrogen crossover and internal current increased with the compression ratio. The diffusion of hydrogen from anode to cathode and the electron transport through the membrane without generating electric power would result in noticeable voltage drops in the OCV [1]. The performance differences among the compression ratios were much larger in the high current density range (>300 mA cm^{-2}) than in the low current density range. As expected, the ohmic resistance generally decreased with the increasing compression ratio, which would have a positive effect on the performance. In the ohmic loss region (~300 to 800 mA cm^{-2}) of the polarization curves, the cell voltage increased to a certain extent with the decreasing ohmic resistance. Out of the ohmic loss region, however, the cell voltage was not directly changed with the compression ratio. This might be due to the effects of the activation and mass-transport losses. In

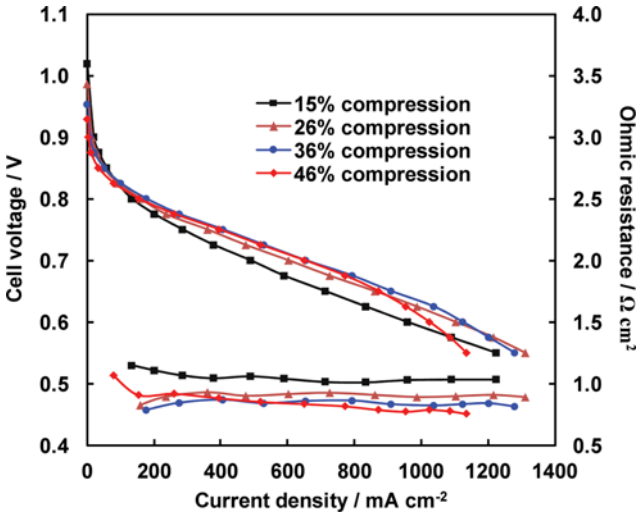

Fig. 2. Polarization curves and ohmic resistances measured at four different compression ratios: 15%, 26%, 36%, and 46%.

the mass-transport region (>800 mA cm^{-2}), the increases in the compression ratio would hinder gas transport and water removal by reducing the pore volume of the GDLs, exerting a negative effect on the performance of the fuel cell.

At the lowest compression ratio (15%), the fuel cell was under-compressed, leading to the much lower cell voltage in the ohmic loss region than the other three compression ratios. In contrast, at the highest compression ratio (46%), the fuel cell was over-compressed, resulting in the sharp voltage drop and deviation from a linear relationship with the current density in the mass-transport loss region. These observations clearly indicate that an optimal compression ratio of the GDLs exists between the two extreme ratios.

2. Effect of GDL Compression on the Over-voltages

The polarization curves shown in Fig. 2 were fitted by using the polarization curve-fitting model described in Eq. (2) to analyze the effect of GDL compression on the performance of the fuel cell by decomposing them into the OCV and the three over-voltages (activation, ohmic, and mass-transport). Fig. 3 shows the fitted polarization curves along with the measured voltages and absolute fitting errors. As can be seen, the fitted voltages almost perfectly matched the measured ones across the current density for all the four compression ratios. The quantitative fitting-performance criteria listed in Table 1 also confirmed the excellence of the fitting-model: the fitting results produced high R^2 (coefficient of determination) values close to 1 and significantly low RMSEs (root-mean-square errors). Therefore, we concluded that the polarization curve-fitting model can be reliably used for the analysis of the GDL compression effects.

Table 1. Fitting-performance criteria calculated from the polarization curve-fitting results

Fitting-performance criteria	GDL compression ratio			
	15%	26%	36%	46%
R^2	0.9998	0.9998	0.9997	0.9998
RMSE (mV)	2.4	2.0	2.6	2.6
Max error (mV)	4.8	4.0	4.4	7.7

The model parameters were estimated from the least-squares fitting of the polarization curves and are summarized in Table 2. From the estimated parameters, the over-voltages for the four compression ratios were calculated at a current density of 1,000 mA cm^{-2}. Fig. 4 plots the OCV and calculated over-voltages against the compression ratio. The OCV almost linearly decreased with the increasing compression ratio (Fig. 4(a)). As explained in the previous section, the OCV dropped with increasing the hydrogen

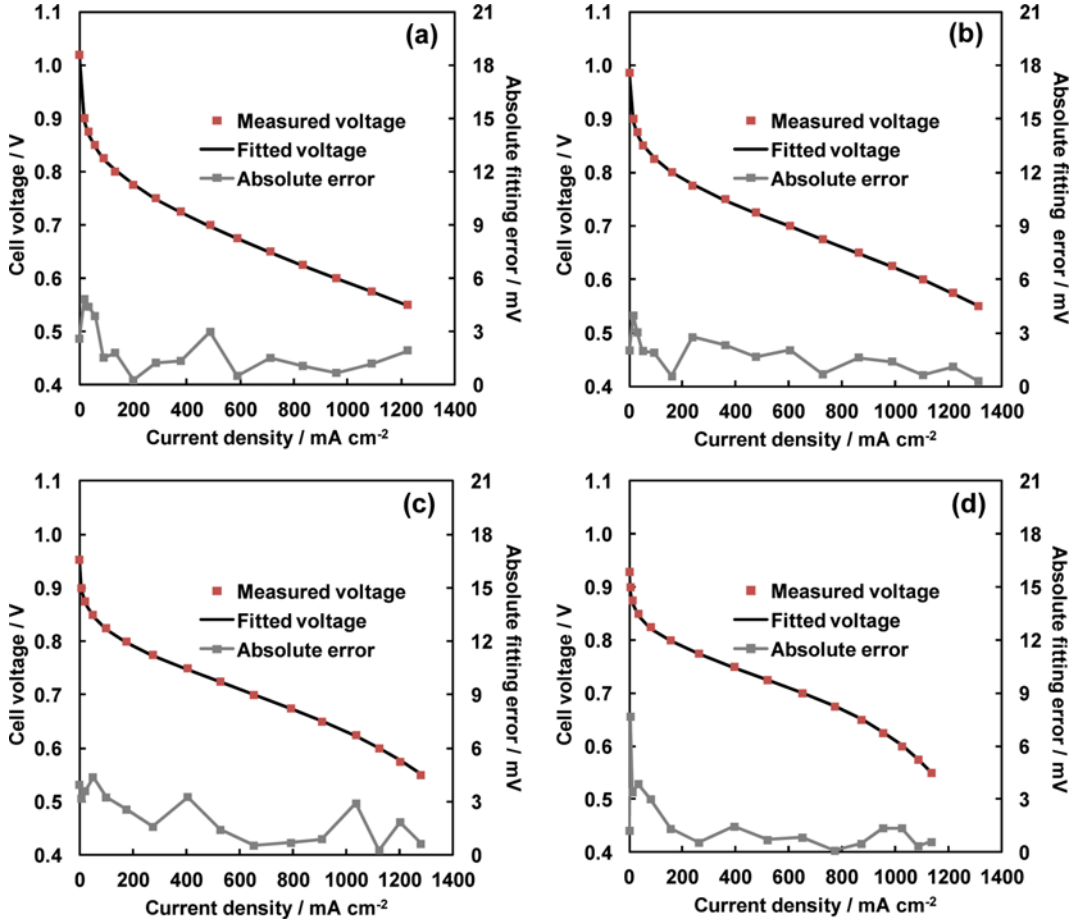

Fig. 3. Comparison of the fitted polarization curves with the measured ones at four different compression ratios: (a) 15%, (b) 26%, (c) 36%, and (d) 46%.

Table 2. Estimated parameters of the polarization curve-fitting model for the polarization curves measured at the four compression ratios

Compression ratio	E_0 (V)	b (V)	R (kΩ cm^2)	p (V)	q (cm^2 mA^{-1})
15%	1.0225	0.04091	1.43×10^{-4}	9.08×10^{-4}	1.83×10^{-3}
26%	0.9889	0.03288	1.25×10^{-4}	8.85×10^{-4}	2.88×10^{-3}
36%	0.9578	0.02667	1.17×10^{-4}	8.41×10^{-4}	3.42×10^{-3}
46%	0.9285	0.02198	1.13×10^{-4}	7.29×10^{-4}	4.29×10^{-3}

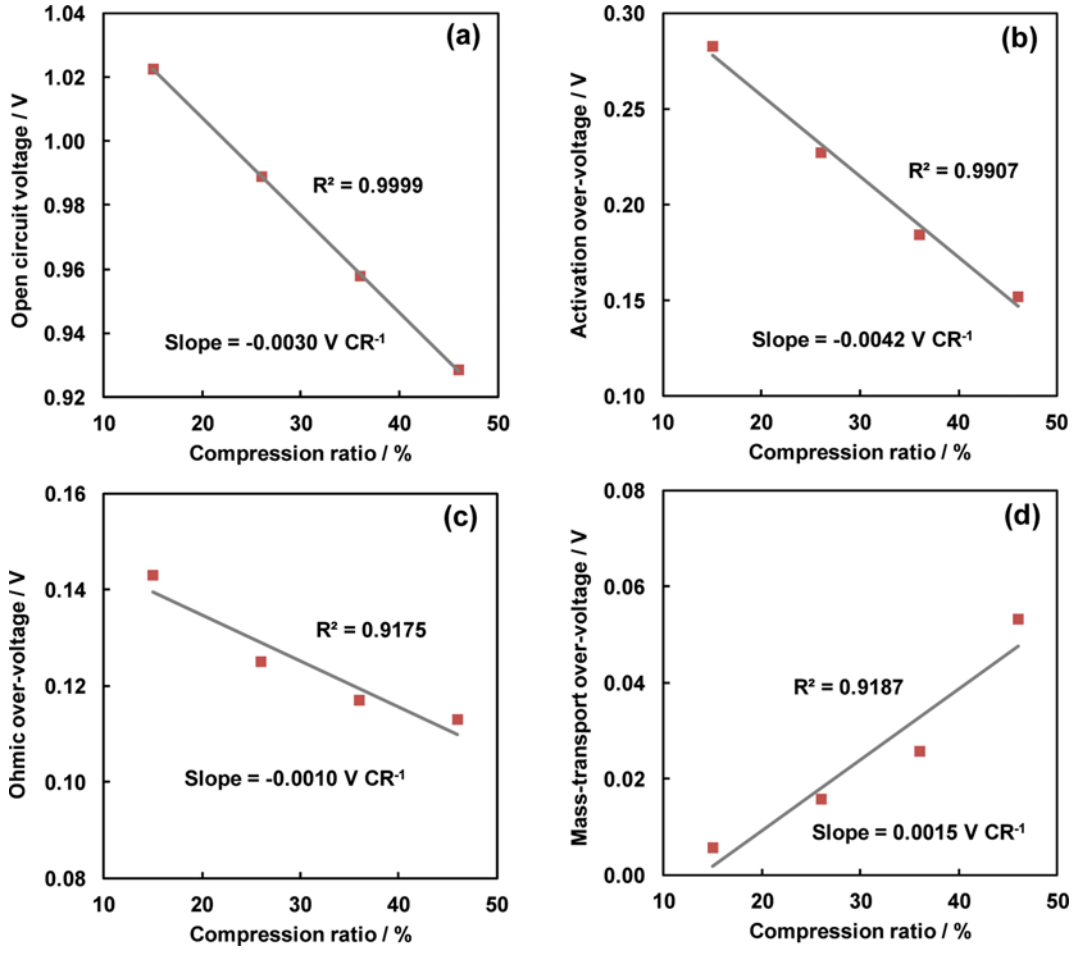

Fig. 4. Plots of the OCV and three over-voltages against the compression ratio (CR): (a) OCV, (b) activation over-voltage, (c) ohmic over-voltage, and (d) mass-transport over-voltage.

crossover and/or internal current in the fuel cell. As shown in Fig. 5, the hydrogen crossover current measured using the LSV clearly confirmed that the hydrogen crossover rate increased with the increasing compression ratio of the GDLs. The increase in the hydrogen crossover rate would result from membrane thinning or minute damages due to the increased compression of the MEA and GDLs. As shown in Figs. 4(b) and 4(c), both the activation and ohmic over-voltages decreased with the compression ratio. In general, an increase in the compression of a PEM fuel cell enlarges the contact area between the cell components. This would increase the real surface area of the electrodes and consequently reduce the activation over-voltage. The contact resistance between the cell components would decrease with the enlarged contact area, thus reducing ohmic over-voltage. As shown in Fig. 4(d), the mass-transport over-voltage increased with the increasing compression ratio. This can be explained by the reduced pore volume of GDLs which increases gas transport resistance and hinders water removal from the catalyst layers. Among the over-voltages that caused voltage drops from the reversible (no loss) voltage, the activation over-voltage was the most severely affected by the compression ratio: the activation over-voltage decreased by 0.0042 V when the compression ratio increased by 1%. The OCV showed the second largest change to the compression ratio (0.0030 V CR^{-1}). Compared with the OCV and the activation over-voltage, the ohmic and mass-transport over-voltages were relatively less affected by the compression ratio (0.0010 V CR^{-1} and 0.0015 V CR^{-1} for the ohmic and mass-transport over-voltages, respectively). Even at the high current density of 1,000 mA cm^{-2}, the activation over-voltage was found to be the

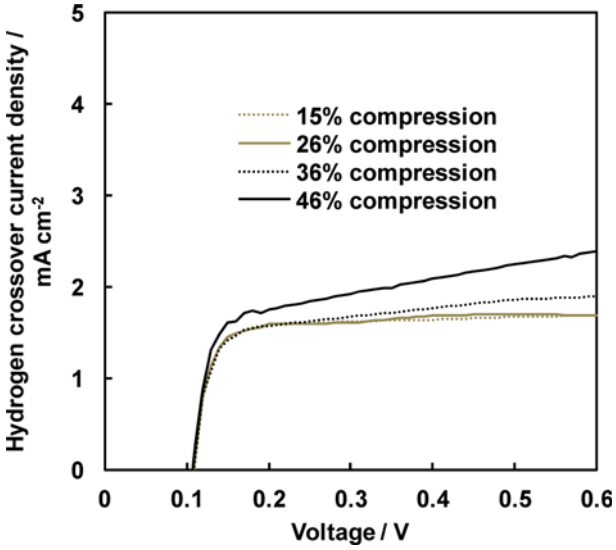

Fig. 5. Hydrogen crossover currents measured using LSV at four different compression ratios: 15%, 26%, 36%, and 46%.

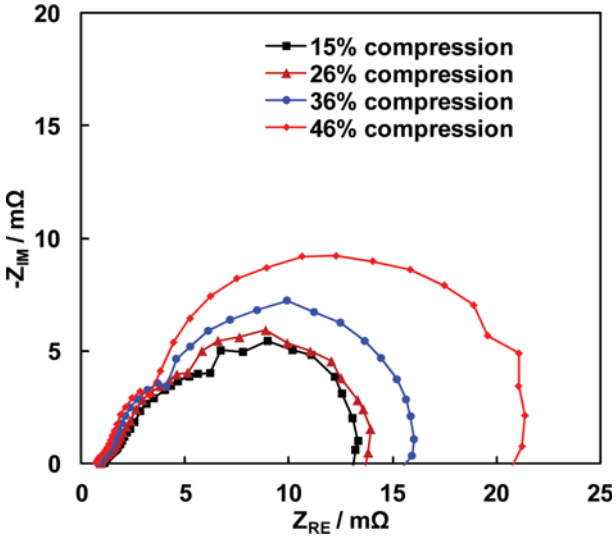

Fig. 6. Nyquist plots of the impedance spectra measured at a current density of 1,000 mA cm^{-2} for the four different compression ratios of 15%, 26%, 36%, and 46%.

dominant factor among the three over-voltages (activation, ohmic, and mass-transport).

Fig. 6 shows the Nyquist plots of the impedance spectra measured at a current density of 1,000 m A^{-2} for the four compression ratios of 15%, 26%, 36%, and 46%. As can be seen, two semicircles partially overlapping with each other appeared for each of the Nyquist plots. The smaller semicircles on the left side of the complex plane account for the charge-transfer resistances, and the larger semicircles on the right side explain the mass-transfer resistances. As a result, the Nyquist plots can be interpreted as follows: both the charge-transfer and ohmic resistances decreased as the compression ratio increased, whereas the mass-transfer resistances increased. This indicates that the analysis results obtained using the proposed polarization curve-fitting model, described in the previous paragraph, are in agreement with the AC impedance measurements.

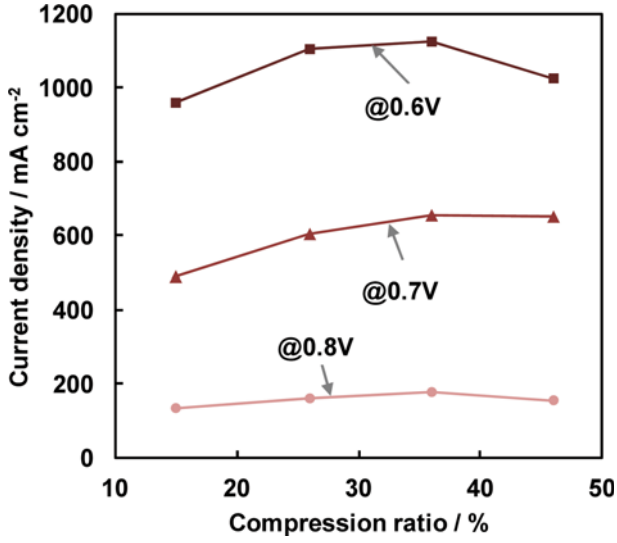

Fig. 7. Plot of the measured current densities against the compression ratio at cell voltages of 0.6, 0.7, and 0.8 V.

3. Optimal Compression of the GDLs

The optimal compression ratio of the GDLs was determined from the measured polarization curves. Fig. 7 plots the current densities measured at cell voltages of 0.6, 0.7, and 0.8 V (PEM fuel cells typically operate in a cell voltage range of 0.6 to 0.8 V) against the compression ratio. As can be seen, the lower the cell voltage, the more sensitive is the current density to the compression ratio. For all the three cell voltages, the maximum points of the current density curves were between the two extreme compression ratios examined in this study, and were found at the compression ratio of 36% among the four compression ratios. If we only focus on the performance of the fuel cell, the optimal compression ratio will be approximately 36%. However, the optimal compression ratio should be set at a somewhat lower value than 36% to consider the durability of the membrane of the fuel cell because the hydrogen crossover rate at 36% was considerably higher than that at 26% (see Fig. 5). It has been well known that the durability of the membrane strongly depends on the hydrogen crossover rate [25,26]. Hydrogen permeating through the membrane can generate hydrogen peroxide (H_2O_2), which is converted to hydroxyl (HO) or peroxide (HOO) radicals. These radicals then attack the membrane, resulting in membrane thinning or pinhole formation. Therefore, the lower the hydrogen crossover rate, the higher is the durability. Long-term operations of the fuel cell under different compression ratios may be necessary to exactly determine the optimal compression ratio that satisfies its desired durability.

CONCLUSIONS

The effect of GDL compression on the polarization curves of a PEM fuel cell was analyzed using a polarization curve-fitting model. The polarization curves of the fuel cell were obtained from single-cell tests at four different compression ratios of the GDLs.

The polarization curves were almost perfectly fitted with the model, and the estimated model parameters were used for the analysis of the effects of GDL compression on the OCV and the over-voltages resulting from activation, ohmic, and mass-transport losses. The analysis results can be summarized as follows: 1) the OCV linearly decreased with the increasing compression ratio of the GDLs; 2) the activation and ohmic over-voltages decreased with the compression ratio, whereas the mass-transport over-voltage increased; and 3) the activation over-voltage and the OCV were significantly affected by the compression ratio, whereas the ohmic and mass-transport over-voltages were relatively less affected. The optimal compression ratio was found at approximately 36% for the maximum performance of the fuel cell and at somewhat less than 36% for higher durability. The proposed analysis method based on the polarization curve-fitting model can be applied to identifying quantitative differences of polarization curves obtained under various operating conditions and designs for fuel cells.

REFERENCES

1. J. Larminie and A. Dicks, *Fuel cell systems explained*, 2nd Ed., Wiley, West Sussex, England (2003).
2. F. Barbir, *PEM fuel cells: Theory and practice*, 2nd Ed., Elsevier, Burlington, USA (2013).
3. Y. Wang, K. S. Chen, J. Mishler, S. C. Cho and X. C. Adroher, *Appl. Energy*, **88**, 981 (2011).
4. I.-S. Han and H. K. Shin, *Korean Chem. Eng. Res.*, **53**, 236 (2015).
5. A. Mendez, T. J. Leo and M. A. Herreros, *Energies*, **7**, 4676 (2014).
6. S. Park and B. N. Popov, *Korean J. Chem. Eng.*, **31**, 1384 (2014).
7. I.-S. Han, B.-K. Kho and S. Cho, *J. Power Sources*, **304**, 244 (2016).
8. C. H. Choi, S. Yu, I.-S. Han, B.-K. Kho, D.-G. Kang, H. Y. Lee, M.-S. Seo, J.-W. Kong, G. Kim, J.-W. Ahn, S.-K. Park, D.-W. Jang, J. H. Lee and M. Kim, *Int. J. Hydrogen Energy*, **41**, 3591 (2016).
9. W.-K. Lee, C.-H. Ho, J. W. Van Zee and M. Murthy, *J. Power Sources*, **84**, 45 (1999).
10. J. Ge, A. Higier and H. Liu, *J. Power Sources*, **159**, 922 (2006).
11. J.-H. Lin, W.-H. Chen, Y.-J. Su and T.-H. Ko, *Fuel*, **87**, 2420 (2008).
12. Y. Zhou, K. Jiao, Q. Du, Y. Yin and X. Li, *Int. J. Hydrogen Energy*, **38**, 12891 (2013).
13. I. Nitta, O. Himanen and M. Mikkola, *Electrochem. Commun.*, **10**, 47 (2008).
14. M. S. Ismail, D. B. Ingham, L. Ma and M. Pourkashanian, *Renew. Energy*, **52**, 40 (2013).
15. D. Ye, E. Gauthier, J. B. Benziger and M. Pan, *J. Power Sources*, **256**, 449 (2014).
16. A. Bazylak, D. Sinton, Z.-S. Liu and N. Djilali, *J. Power Sources*, **163**, 784 (2007).
17. D. H. Yee, E. Gauthier, M. J. Cheah, J. Benziger and M. Pan, *AIChE J.*, **61**, 355 (2015).
18. X. Yuan, H. Wang, J. C. Sun and J. Zhang, *Int. J. Hydrogen Energy*, **32**, 4365 (2007).
19. S. Haji, *Renew. Energy*, **36**, 451 (2011).
20. M. V. Moreira and G. E. da Silva, *Renew. Energy*, **34**, 1734 (2009).
21. J. Kim, S.-M. Lee, S. Srinivasan and C. E. Chamberlin, *J. Electrochem. Soc.*, **142**, 2670 (1995).
22. A. Saadi, M. Becherif, A. Aboubou and M. Y. Ayad, *Renew. Energy*, **56**, 67 (2013).
23. F. Laurencelle, R. Chahine, J. Hamelin, K. Agbossou, M. Fournier, T. K. Bose and A. Laperriere, *Fuel Cells*, **1**, 66 (2001).
24. MATLAB optimization toolbox user's guide, http://it.mathworks.com/help/pdf_doc/optim/optim_tb.pdf.
25. M. Inaba, T. Kinumoto, M. Kiriake, R. Umebayashi, A. Tasaka and Z. Ogumi, *Electrochim. Acta*, **51**, 5746 (2006).
26. X.-X. Yuan, S. Zhang, H. Wang, J. Wu, J. C. Sun, R. Hiesgen, K. A. Friedrich, M. Shulze and A. Huag, *J. Power Sources*, **195**, 7594 (2010).